Annual Report, 1998

3D Elastic Finite Difference Simulation of a Dynamic Rupture (SCEC Group G)

Investigators: Dr. Kim B. Olsen, Institute for Crustal Studies, UC Santa Barbara

These results have been obtained in collaboration with Dr. Raul Madariaga, Ecole Normale Superieure, Paris, and Dr. Stefan Nielsen.

Rupture initiation and propagation in a homogeneous stress field.

We have studied rupture growth on a simple flat fault embedded in a homogeneous elastic medium of rigidity μ, using the dynamic boundary conditions presented by Madariaga et al. (1998) and used by Olsen et al. (1997). Our results show a simple scaling of the rupture as a function of slip-weakening distance, asperity size, and grid size (Figure 1). The degree of resolution improves as D_0 increases, and we find that numerical simulations are stable and reproducible for $D_0 > 4$. Rupture initiation is controlled by non-dimensional ia number

$$\lambda = \frac{T_e^2}{\mu T_u} \frac{R}{D_0} \tag{1}$$

where R is the patch (asperity) radius, T_e is a characteristic stress load on this patch and $T_u \times D_0$ is a measure of the energy release rate on the fault. A similar non-dimensional coefficient was first proposed by Andrews (1976) in a somewhat different context.

An essential requirement for rupture to grow beyond the asperity is that $\lambda > \lambda_c$ where λ_c is a critical value of λ for the circular asperity. λ_c defines a bifurcation of the problem as a function of parameter λ. For $\lambda < \lambda_c$ rupture does not grow beyond the initial asperity. For $\lambda > \lambda_c$ rupture grows indefinitely at increasing speed (Figure 2). This is a simple example of a pitch-fork bifurcation, with one complication: if the parameter $\lambda > 1.3\lambda_c$ the rupture front in the in-plane direction jumps ahead to speeds higher that for the shear wave speed. The rupture front acquires an elliptical shape elongated along the in-plane direction (see Figure 1).

As for rupture initiation, rupture propagation is controlled by a non-dimensional number

$$\kappa = \frac{T_e^2}{\mu T_u} \frac{W}{D_0} \tag{2}$$

where W is the width of the fault. Ruptures stop for low values $\kappa < \kappa_c$ and grow indefinitely for $\kappa > \kappa_c$. Again for a certain value of $\kappa > 1.2\kappa_c$ ruptures grow initially at very high speeds and then jump to a speed higher than the shear wave velocity.

Rupture initiation and propagation in a heterogeneous stress field: the Landers earthquake.

We have followed up on the dynamic simulations of the Landers earthquake by Olsen et al. (1997). Here, we also used a small asperity meeting condition (1) at the southern end of the causative fault to initiate a spontaneous rupture. Using a simple slip-weakening friction law and a heterogeneous prestress distribution computed similarly to that by Olsen et al. (1997) we have analyzed the sensitivity of the rupture to the choice of tectonic stress (a constant contribution to the prestress due to tectonic forces), yield stress, and a spatially-invariant slip weakening parameter (Figure 3).

The moment increases with larger values of tectonic stress, yield stress, and smaller slip weakening distance, for combinations of these parameters that allow rupture. The duration increases with the slip weakening distance. Figure 3 shows that only the product of the slip weakening distance and the yield stress is constrained, or in other words, the rupture energy, $\frac{1}{2}T_u D_0$. Figure 3 suggests that combinations of the parameters with rupture energy in the range 5-20 MJ/m^2 provide a moment ($> 5.0e^{19}Nm$) and duration ($>$ 18 s) in closest agreement with those from the kinematic analyses of the Landers earthquake.

3D dynamic simulations of dipping faults: the Northridge earthquake

Here we use an alternative mixed boundary condition with numerical accuracy possibly superior to that by Madariaga et al. (1998) which has been implemented in the 3D elastic finite-difference code in collaboration with Dr. Stefan Nielsen (Nielsen and Olsen, 1998, 1999). In this code we have implemented a dipping free-surface condition, which was used to simulate the 1994 Northridge earthquake in a similar fashion to the procedure used by Olsen et al. (1997) for the Landers earthquake. We implemented a dipping free-surface boundary condition using the void (vacuum) formulation, and kept the fault aligned with one of the grid planes. The prestress distribution is computed from the kinematic slip distribution by Wald et al. (1996). We used a yield stress of 100 bars, a slip weakening distance of 20 cm, and a rate weakening distance of 5 cm/s. Snapshots of the dynamic rupture is shown in Figure 4, and the final slip distribution, which is a smooth version of that used to compute the prestress, is shown in Figure 5.

References and SCEC publications

Andrews, J. (1976). Rupture velocity of plane strain shear cracks, *J. Geophys. Res.* **81**, 5679-5687.

Carlson, J.M, S. Nielsen, and K.B. Olsen (1998). Friction laws and fault models, *EOS*, Transactions, supplement, **79**, F635.

Madariaga, R., and K.B. Olsen (1999). Scaling criteria for dynamic ruptures in a 3-D elastic medium, in preparation.

Madariaga, R., K.B. Olsen, and R.J. Archuleta (1998). Modeling dynamic rupture in a 3D earthquake fault model, *Bull. Seism. Soc. Am.* **88**, 1182-1197.

Nielsen, S.B., and K.B. Olsen (1998). A mixed boundary condition for rupture dynamics in finite difference simulations, submitted to *Geophys. Res. Lett.*

Nielsen, S.B., and K.B. Olsen (1998). A mixed boundary condition for rupture dynamics in finite difference simulations, *EOS*, Transactions, supplement, **79**, F631.

Olsen, K.B. and R. Madariaga (1998). Constraining the rupture dynamics for the 1992 landers earthquake using kinematic wave propagation, *EOS*, Transactions, supplement, **79**, F609.

Olsen, K.B., R. Madariaga, and R.J. Archuleta (1997). Three-Dimensional dynamic simulation of the 1992 Landers Earthquake, *Science* **278**, 834-838.

Wald, D.J., T.H. Heaton, and K.W. Hudnut (1996). The slip history of the 1994 Northridge, California, Earthquake determined from strong-motion, teleseismic, GPS, and leveling data, *Bull. Seis. Soc. Am.* **86**, S49-S70.

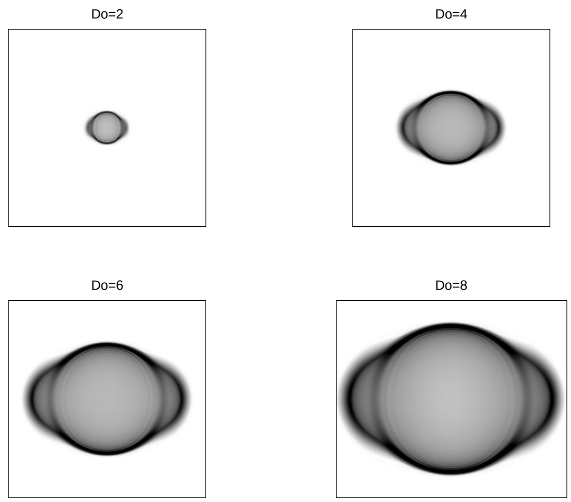

Figure 1: Scaling of rupture at constant load for spontaneous rupture starting from an overloaded asperity. The four snapshots show the distribution of slip rate on the fault at equivalent times for four different values of D_0 and the initial asperity radius R (top left) $D_0 = 2$, $R = 3$ and $T = 140$; (upper right) $D_0 = 4$, $R = 6$ and $T = 280$; (bottom left) $D_0 = 6$, $R = 9$ and $T = 420$; and (bottom right) $D_0 = 8$, $R = 12$ and $T = 560$.

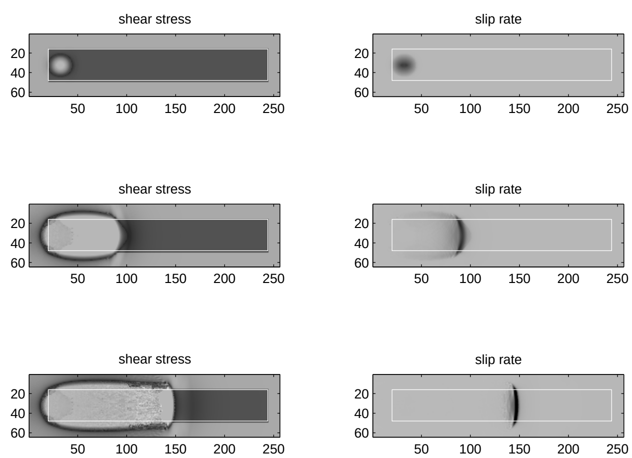

Figure 2: Snapshots of the shear stress and slip rate fields on a fault containing a very long and narrow asperity (yellow in the stress snapshots). The top panels show ruptures at sub-critical, slightly super critical and super critical values of the parameter λ.

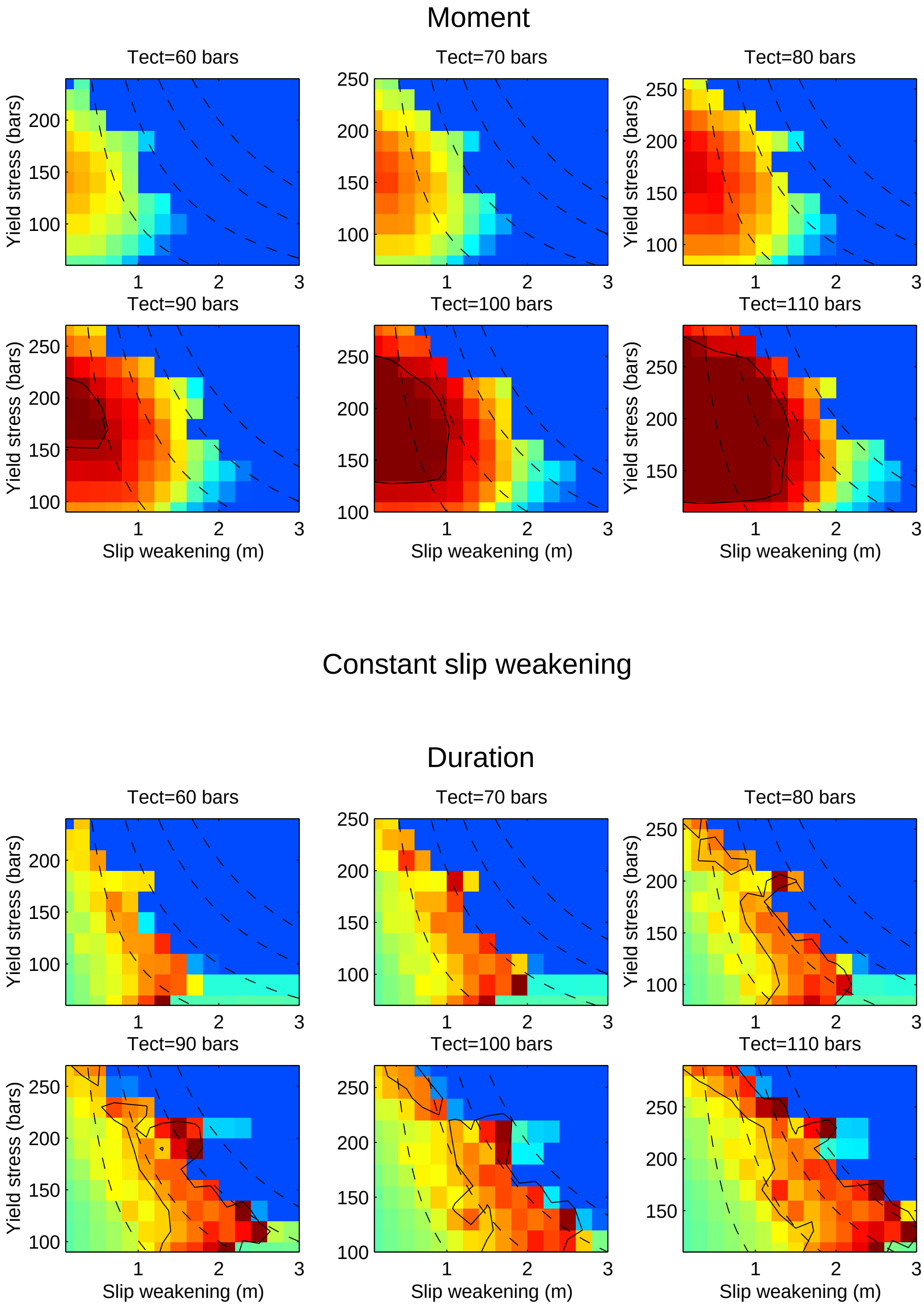

Figure 3: Moment and duration as a function of tectonic stress, yield stress, and slip weakening. The solid contour lines depict values of $5.0e^{1}9$ Nm for the moment, and 18 seconds for the duration plots. The dashed lines depict rupture energy release of 5, 10, 15 and 20 MJ/m^2

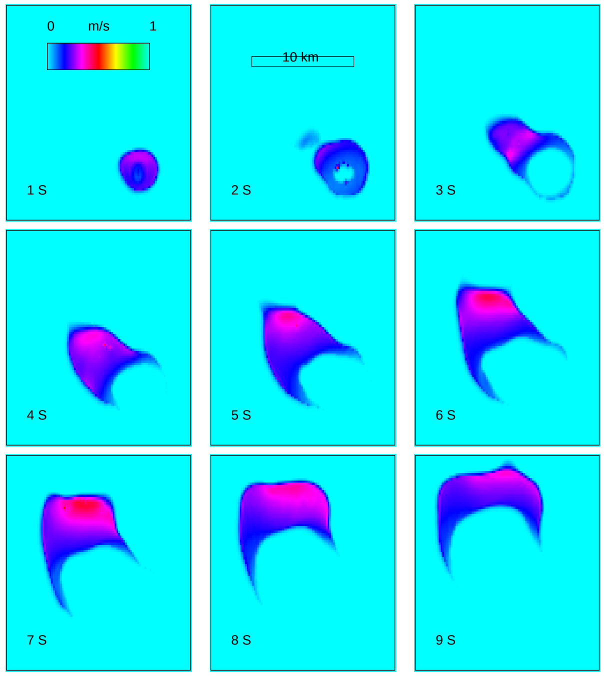

Figure 4: Snapshots of the sliprate from our dynamic simulation of the Northridge earthquake. We used a slip weakening distance of 20 cm, a rate weakening velocity of 5 cm/s and a yield stress of 100 bars. The prestress was constrained to values just below the yield stress to prevent rupture initiation from several locations on the fault. The rupture was initiated from a small asperity at the hypocenter depicted from data.

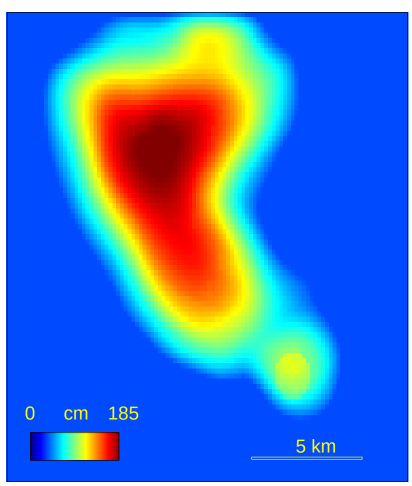

Figure 5: Final slip distribution from the dynamic Northridge simulation.